Correlated Link Shadow Fading in Multi-hop Wireless Networks

Piyush Agrawal, *Student Member, IEEE,* and Neal Patwari, *Member, IEEE,*

***Abstract*—Accurate representation of the physical layer is required for analysis and simulation of multi-hop networking in sensor, ad hoc, and mesh networks. Radio links that are geographically proximate often experience similar environmental shadowing effects and thus have correlated shadowing. This paper presents and analyzes a non-site-specific statistical propagation model which accounts for the correlations that exist in shadow fading between links in multi-hop networks. We describe two measurement campaigns to measure a large number of multi-hop networks in an ensemble of environments. The measurements show statistically significant correlations among shadowing experienced on different links in the network, with correlation coefficients up to 0.33. Finally, we analyze multi-hop paths in three and four node networks using both correlated and independent shadowing models and show that independent shadowing models can underestimate the probability of route failure by a factor of two or greater.**

***Index Terms*—Wireless sensor, ad hoc, mesh networks, shadowing, correlation, statistical channel model, wireless communication, measurement, performance**

I. Introduction

Both simulation and analysis are critical to the development of multi-hop networks, including mesh, ad-hoc, and sensor networks. However, current physical layer models do not accurately represent radio channels in multi-hop wireless networks [1], [2]. As a result, there is a significant disconnect between simulation and analysis, and real world deployment. There is a significant interest in improving statistical models beyond the current state-of-the-art, in order to decrease the difference between simulation and analysis results and experimental deployment results.

Path losses between pairs of nodes are critical in any simulation or analysis of a multi-hop network. Path losses determine the connectivity and performance of multi-hop wireless networks. Path loss between an interferer and receiver determines the received interference power, which determines whether communication can exist during transmission of interference. In power control schemes, path losses between pairs of nodes determine the energy consumption required for communication between the nodes. In received signal strength (RSS)-based localization, path losses determine the errors in range and position estimates of nodes.

This paper presents a non-site-specific statistical joint path loss model between a set of static nodes. Current statistical channel models used for multi-hop networks consider link path losses to be independent. This is a simplifying assumption, since shadow fading is determined by environmental obstructions, and geographically proximate links pass through similar obstructions. We hypothesize that links which pass through nearby parts of the environment have correlated shadowing losses. In this paper, we conduct extensive measurements to verify this hypothesis.

Non-site-specific path loss models are critical for multi-hop network analysis and simulation. Site-specific models use building floor plans or maps of the particular deployment area to predict path losses in the network, and have been critical for deployment planning for cellular systems and large WLAN deployments [3], [4]. However, site-specific models are not valuable for determining the statistical performance of a wireless network across the ensemble of possible deployments. Non-site-specific path loss models, often referred to simply as statistical path loss models, help system designers understand how network performance improves or degrades based on design decisions, in general environments.

A. Single-Link Path Loss Model

Radio propagation measurement and modeling for a single radio link has been reported extensively over the past century [5], [6], [7], [8]. In general, when there is no site-specific knowledge of the environment, the ensemble mean received power, $\bar{P}(d)$ (dBm), at a distance d from the transmitter, is [6], [7],

$$\bar{P}(d) = P_T - \Pi_0 - 10n_p \log_{10} \frac{d}{\Delta_0}, \tag{1}$$

where P_T is the transmitted power in dBm, n_p is the path loss exponent, and Π_0 is the loss experienced at a short reference distance Δ_0 from the transmitter antenna. This model incorporates the free space path loss model when $n_p = 2$, and extends to practical (obstructed) multipath environments when $n_p > 2$.

On a particular link, received power will vary from the ensemble mean because of *fading*. The measured received power for the link between transmitter i and receiver j can be written as,

$$P_{i,j} = \bar{P}(d_{i,j}) - Z_{i,j}, \tag{2}$$

where, $d_{i,j}$ is the distance between nodes i and j, and $Z_{i,j}$ is the fading loss. In general, shadow fading, narrowband or frequency-selective fading, and antenna and device losses all contribute to $Z_{i,j}$. Much research in antennas and propagation, and in RFIC design, have developed models for losses due to narrowband fading, antenna and device losses. Two antennas

The manuscript was received on November 19, 2007, and revised on October 20, 2008. The associate editor coordinating the review of this paper and accepting it for publication was Dr. Rohit Nabar.

P. Agrawal and N. Patwari are with the department of Electrical and Computer Engineering, University of Utah, Salt Lake City, UT 84112.

spaced closer than a wavelength do experience correlated small-scale fading, and a large body of research has explored those correlations [9].

This paper models the correlations among shadow fading on the various links in a network. Shadow fading, also called medium-scale fading [6], describes the loss experienced as the signal passes through or diffracts around major obstructions in its path from the transmitter to the receiver. These obstructions include walls and furniture indoors, and buildings, terrain, and trees outdoors.

We hypothesize that shadowing losses on different links are correlated when those links are geographically proximate. Since shadowing is central to the analysis in this paper, we separate total fading loss $Z_{i,j}$ into two components,

$$Z_{i,j} = X_{i,j} + Y_{i,j}, \tag{3}$$

where $X_{i,j}$ represents the shadow fading loss, and $Y_{i,j}$ represents all other (non-shadowing) losses.

B. Application in Multi-hop Networking Research

In the multi-hop networking simulation and analysis literature, two path loss models are used:

1) The circular coverage model: $Z_{i,j} = 0$ for all links, and thus the coverage area is a perfect circle, as shown in Figure 1(a).
2) The i.i.d. log-normal shadowing model: For all links (i, j), random variables $Z_{i,j}$ (in dB) are independent and identically distributed Gaussian with zero mean and variance σ_Z^2, as shown in Figure 1(c).

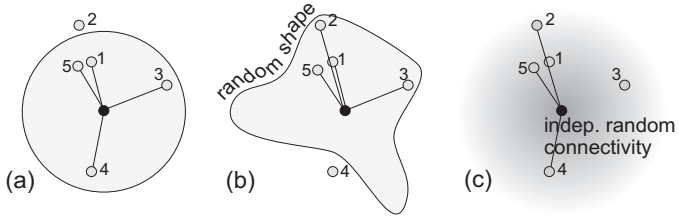

Fig. 1. Graphical depiction of (a) circular coverage model, and (c) coverage in the i.i.d. log-normal shadowing model, compared to the common depiction of (b) in which coverage area is a random shape. In (a) and (b), nodes are connected if and only if they are within the gray area, while in (c), nodes are connected with probability proportional to the shade (darker is more probable).

We argue that the two models are at opposite extremes, and both problematic. Note that 'realistic coverage' is commonly depicted pictorially as a coverage area with random range as a function of angle [10], [11], as in Figure 1(b), and neither fading model produces such a random shape. It is easy to recognize that the deterministic, circular coverage areas are unrealistic for wireless communications links. However, circular coverage has been a common assumption in ad hoc and sensor network research and has been used to generate foundational research results. It has been shown that the majority of papers which require radio propagation models in their simulation use the circular coverage model [12].

In comparison, the i.i.d. shadowing model eliminates the concept of coverage area. Since the model has no spatial memory, even two nearly overlapping links would be represented as statistically independent. For example node 2 in Figure 1(c) may be connected while node 1 is not.

Recent research, including Hekmat and Van Mieghem [11] and Bettstetter and Hartmann [10], has studied connectivity in ad hoc networks using the i.i.d. log-normal shadowing model. Their analyses indicate that for a constant level of connectivity, node deployment density can be reduced when the variance of the shadowing is increased. This increase in connectivity is largely a result of the model's independence assumption. Since losses in links in the same direction from a transmitter are independent, if one link is disconnected because of high loss, another node in the same direction is likely to be connected.

In reality, if an obstacle in one direction from a transmitter strongly attenuates its signal, any receiver behind the obstacle is likely to experience high fading loss. For example, if the environment in Figure 2 causes severe shadowing, it is likely to cause additional path loss on both links a and b. In contrast, the i.i.d. log-normal shadowing model assumes that the shadowing across links a and b will be independent and thus exaggerate the connectivity. We quantify this argument in Section VI.

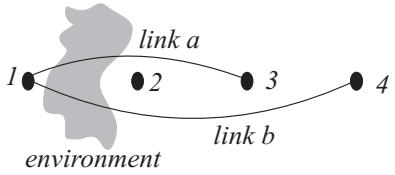

Fig. 2. Example of factor in shadowing loss correlation. Because link a and link b cross the same environment, their shadowing losses tend to be correlated.

C. Correlation Limits Link Diversity

Diversity methods are common means to achieve reliability in unreliable channels. Multi-hop networking serves as a network-layer diversity scheme by allowing two nodes to be connected by any one of several multi-hop paths. All diversity schemes are limited by channel correlations. Correlations have been studied and shown to limit diversity gains in time, space, frequency and multipath diversity schemes [9], [6], [7], [13].

Yet little research has addressed fading correlations among links in sensor, mesh, and ad hoc networks. This paper presents an investigation into quantifying the correlation in the shadow fading experienced on the different links of a multi-hop network, as well as a statistical joint path loss model which represents correlations in link shadowing. This investigation is based on extensive experimental measurements, using full link measurements of an ensemble of deployed networks to estimate and test for statistical correlations. Further, we quantify the effect that such correlation has on source-to-destination path statistics. We show for a simple three node network that the probability of path failure can be double or more what would be predicted by the i.i.d. log-normal shadowing model.

II. Related Research

Shadow fading correlations have been measured and shown to be significant in other wireless networks. For example:

1) In digital broadcasting, links between multiple broadcast antennas to a single receiver have correlated shadowing which affects the coverage area and interference characteristics [14].
2) In indoor WLANs correlated shadowing is significant (with correlation coefficients as high as 0.95), and strongly impacts system performance [15].
3) In cellular radio, correlation on links between a mobile station (MS) and multiple base stations (BSs) significantly affects mobile hand-off probabilities and co-channel interference ratios [16], [17], [18].

In cellular radio, the model of Gudmundson [19] is used to predict shadowing correlation for the link between a mobile station MS to a BS over time as the MS moves. In Section III, we address the inability of this model to be directly applied to model the correlations among links in multi-hop networks. Wang, Tameh, and Nix [20] extended Gudmundson's model to the case of simultaneous mobility of both ends of the link, for use in MANETs, and relate a sun-of-sinusoids method to generate realizations of the shadowing process in simulation. Both works use "correlated shadowing" to refer to the correlation of path loss in a *single link* over time, while the present work studies the correlation of *many disparate links* at a single time.

In [21], RSS measurements in a single network were used to quantify fading correlations between two links with a common node. Those results could not be complete because a single measured network does not provide information about an ensemble of network deployments. The present study uses the data from two campaigns each consisting of multiple measured networks to examine many pairs of links with the identical geometry, both with and without a common node.

Finally, we note that the performance of other RSS-based applications in wireless networks depend on accurate joint path loss models. Cooperative localization in sensor and ad hoc networks uses signal strength to estimate node coordinates. The error performance of such estimators is dependent on the statistical model for path losses in the network. All previous analytical studies of location estimation bounds assume independence of links [22], [23], [24], [25], [26], but new work shows that bounds change when correlated shadowing is taken into account [27]. Further, because multiple links will measure the shadowing caused by an attenuating object, the location of an attenuating object can be estimated. We have shown that tomographic imaging can be used to estimate and track the location of a moving RF attenuator such as a person [27]. Accurate RF tomographic imaging requires a non-site-specific statistical model which relates the attenuation field to the shadowing losses measured on links. This paper presents such a model, and more critically, provides experimental measurements which justify such a model.

III. Motivation

The present effort to model the shadowing correlation is motivated by the fact that no existing correlated link shadowing model is valid for arbitrary pairs of links in ad-hoc networks. Yet shadowing correlation plays a very important role in determing the realistic performance of a network. To date, there have been two relevant statistical models for shadowing correlations:

1) The model of Gudmundson (1991), which predicts temporal shadowing correlations for the MS-BS path loss as the MS moves in a cellular network [19].
2) The model of Wang, Tameh and Nix (2006), an extension of Gudmundson's model, which predicts temporal shadowing correlations on a single link when there is mobility on both ends of the link [20].

In this section, we show that neither model can be applied to model shadowing correlation between arbitrary pairs of links in multi-hop networks.

Gudmundson's model has been widely applied to predict shadowing correlations in cellular networks where a mobile receiver (with a low antenna) communicates with a base station (with a high antenna). The model predicts the correlation in shadowing as the mobile receiver changes position with respect to the base station as shown in Fig. 3. For a mobile receiver going from position $\mathbf{x}_i$ to $\mathbf{x}_j$, the shadowing correlation $R_X(\mathbf{x}_i, \mathbf{x}_j)$ is given as,

$$R_X(\mathbf{x}_i, \mathbf{x}_j) = \sigma_X^2 e^{-d_{ij}/\mathrm{D}} \quad \text{where } d_{ij} = \|\mathbf{x}_i - \mathbf{x}_j\|, \qquad (4)$$

and D is a distance constant, and σ_X^2 is the variance of shadow fading.

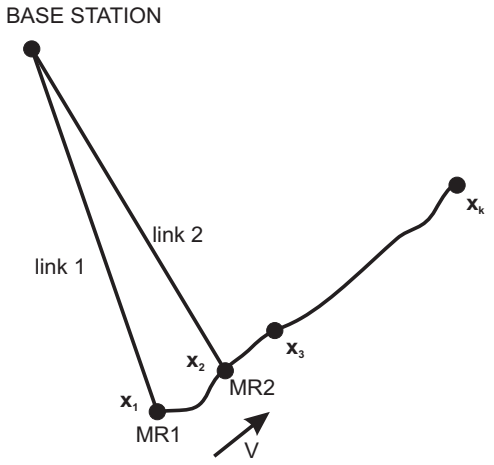

Fig. 3. Example of the motion of mobile receiver and base station position in Gudmundson's model

By design, the Gudmundson model does not apply to pairs of links that do not have a common end point. For example, consider a four node ad-hoc network as shown in Fig. 4. The shadow fading on links c and f have no specified covariance in the model. In typical multi-hop networks with large numbers of nodes, such link pairs occur very commonly – most pairs of links do not share a common node.

A. Adaptation to Mobile-to-Mobile Link

Wang, Tameh, and Nix adapted the Gudmundson model to a more generalized setting of one link with two mobile nodes [20]. Let d_t and d_r be the distance moved the two mobile nodes between two time instants. According to [20],

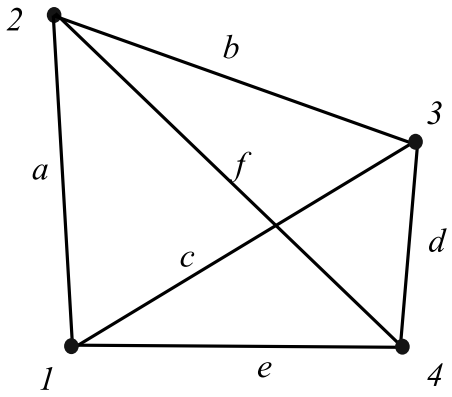

Fig. 4. A simple four node ad-hoc network its six pairwise links.

the correlation between the shadow fading between the two times is modified from (4) to be, $R_X(d_t, d_r) = \sigma_X^2 e^{-\frac{d_t+d_r}{D}}$.

However, the model is based on the assumption that the distances between the two nodes is large compared with d_t and d_r. The model cannot be directly applied to model the covariance of two arbitrary links. We might consider applying [20] to *two* links if those two links share very nearby end points. For example, in Fig. 4, if $d_{23} << d_{12}$ and $d_{14} << d_{12}$, one might use [20] to model the correlation between the shadowing on links a and d.

In general, very few link pairs in ad-hoc networks would meet the above criteria. For example, if d_{23}, d_{24}, d_{13}, d_{14} are of the same order of magnitude as d_{12} and d_{34}, then there is an ambiguity for which two distances should be used in the model of [20]. There seems to be no universally appropriate way to choose the two distances from the four available.

B. Adaptation to Multiple Links

In this section, we introduce what would be the direct application of the Gudmundson (1991) model to an arbitrary set of links in a multi-hop network and show that it does not provide a valid statistical joint path loss model. First, we define a direct, naïve application of (4) to a general multi-link network. For two links $a = (i, j)$ and $b = (k, l)$, the covariance between the shadowing on links a and b would be given by,

$$C(a,b) = \begin{cases} 0, & \text{if } i \neq k, i \neq l, j \neq k, \text{and } j \neq l \\ \sigma_X^2 e^{-d_{ik}/D}, & \text{if } j = l \end{cases} \tag{5}$$

where d_{ik} is the distance between the non-common end points of the two links a and b.

Next, we prove by contradiction that such a model does *not* guarantee a positive semi-definite covariance matrix and thus is not a valid statistical model. Consider the four nodes and the six links between them depicted in Fig. 4. For simplicity, consider a subset of the links, the three links a, d, and e. The covariance matrix for the shadow fading experienced on these three links is given by (5) as,

$$C = \sigma_X^2 \begin{bmatrix} 1 & 0 & e^{-d_{24}/D} \\ 0 & 1 & e^{-d_{13}/D} \\ e^{-d_{24}/D} & e^{-d_{13}/D} & 1 \end{bmatrix} \tag{6}$$

The determinant of this covariance matrix is,

$$\text{Det}(C) = \sigma_X^2(1 - e^{-2d_{13}/D} - e^{-2d_{24}/D}).$$

When d_{13} and d_{24} are low, $\text{Det}(C) < 0$. A negative determinant shows that C is not positive semi-definite and thus cannot be a valid covariance matrix. Thus the Gudmundson covariance model cannot be directly applied to arbitrary sets of links in a network.

C. Summary

In this section, we have explored application of the shadowing covariance models proposed in [19] and [20] to arbitrary sets of links in wireless networks. We have shown that neither can be applied directly to any general set of links. The Gudmundson model does not consider link pairs that do not have a common endpoint. The adaptation proposed in [20] when both the ends of a link are mobile cannot be applied directly to ad-hoc networks as there would be an ambiguity in which two distances to use in the covariance function. We proved by counterexample that a naïve application of the Gudmundson model to model joint path losses in a multi-link network does not guarantee a valid covariance matrix. These arguments necessitate the development of new statistical path loss model which jointly models multiple links in a mesh, sensor, or ad hoc network.

IV. Joint Path Loss Model

In this section, we propose a statistical joint path loss model for arbitrary sets of links in a wireless network. As described in Section III, existing path loss models are not adequate to model correlations which exist in shadow fading between pairs of links in a network. We provide such a model in this section by connecting path losses in a network to a random shadowing environment of deployment. By connecting path losses to an environment, we preserve the physical relationships which exist between links in real-world deployments. By making the environment random, we preserve the non-site-specific nature of the model and allow it to be used in general-purpose simulation and analysis.

We start with the assumption that shadowing losses experienced on the links in a network are a result of an *underlying spatial loss field* $p(\mathbf{x})$. A spatial loss field quantifies the shadowing loss experienced by a link which passes through it – shadowing on a link increases when its path crosses areas of high loss $p(\mathbf{x})$. First, we assume and justify a model for the spatial loss field. We then specify the functional relationship between the random spatial loss field $p(\mathbf{x})$ and path losses below in (9). Finally, we show how this model results in agreement with existing path loss models when considering a single link, and how it models correlated shadowing losses when considering multiple network links.

A. Spatial Loss Field

A statistical model for the spatial loss field $p(\mathbf{x})$ is required for the proposed joint path loss model. We first introduce such a field model and then justify our choices. We assume

that the underlying spatial loss field $p(\mathbf{x})$ is an isotropic wide-sense stationary Gaussian random field with zero mean and exponentially-decaying spatial correlation. The covariance between $p(\cdot)$ at arbitrary positions $\mathbf{x}_i$ and $\mathbf{x}_j$ is given by,

$$\begin{aligned} E\left[p(\mathbf{x}_i)p(\mathbf{x}_j)\right] &= R_p(\mathbf{x}_i,\mathbf{x}_j) = R_p(\|\mathbf{x}_j-\mathbf{x}_i\|) \\ &= \frac{\sigma_X^2}{\delta}\exp\left(-\frac{\|\mathbf{x}_j-\mathbf{x}_i\|}{\delta}\right). \end{aligned} \quad (7)$$

where $\|\mathbf{x}_j-\mathbf{x}_i\|$ is the Euclidian distance between $\mathbf{x}_i$ and $\mathbf{x}_j$, δ is a space constant and σ_X is the standard deviation of the shadow fading. One realization of the random field $p(\mathbf{x})$ is shown in Fig. 5.

The use of a zero-mean Gaussian random field is justified as follows.

1) A large-scale path loss equation such as (1) removes the mean shadowing loss when parameters Π_0 and n_p are estimated. Thus $Z_{i,j}$ is zero-mean.
2) Shadowing losses are often modeled as Gaussian when expressed in (dB). Our assumption of a Gaussian field results in this desired model property, as discussed below.

Two other assumptions about the statistical properties of $p(\mathbf{x})$ are justified below.

1) Isotropy: The assumption that the covariance between $p(\mathbf{x}_1)$ and $p(\mathbf{x}_2)$ is a function of $\|\mathbf{x}_2-\mathbf{x}_1\|$ is valid when the field $p(\mathbf{x})$ is homogeneous and isotropic, which is suitable for many applications [28], [29]. A particular environment realization may have directional biases, but over an ensemble of environments, we would not expect anisotropy. We note that isotropic field models are the building blocks for more sophisticated non-isotropic and non-stationary fields which might be applied to future models for specific anisotropic environments.

2) Exponential Decaying Covariance: Many mathematically valid spatial covariance functions for isotropic fields are possible [30], [31]. We justify the use of the covariance function in (7) because of its basis in a Poisson spatial random process. Poisson processes are commonly used for modeling the distribution of randomly arranged points in space, and we suppose that attenuating obstructions can be modeled in such a fashion as well. Certainly, particular environments (*e.g.*, buildings in city blocks) have order which is not modeled in a Poisson point process, but a general statistical model should be neither specific to a particular type of environment nor overly complicated for analysis.

Analysis of Poisson point processes leads to an exponentially decaying covariance function. Assume that the attenuating field $p(\mathbf{x})$ is defined as the number of obstructions within a distance $R/2$ of point $\mathbf{x}$. When the obstructions are modeled as a 2-D Poisson process, the covariance, $C(r)$, between two points separated by a distance r can be written as [31],

$$C(r) = \begin{cases} \sigma^2\left[1-\frac{2}{\pi}\left[S(r)+\sin^{-1}\left(\frac{r}{R}\right)\right]\right] & r \le R \\ 0 & r \ge R, \end{cases} \quad (8)$$

where $S(r) = \frac{r}{R}\sqrt{\left(1-\frac{r^2}{R^2}\right)}$ and σ^2 is the variance of the attenuating field $p(\mathbf{x})$, when $r=0$. The behavior of $C(r)$ in (8) is approximately equal to a function with exponential decay in r for low r [31]. We propose, for simplicity, to use an exponentially-decaying covariance function of (7) to describe the spatial loss field.

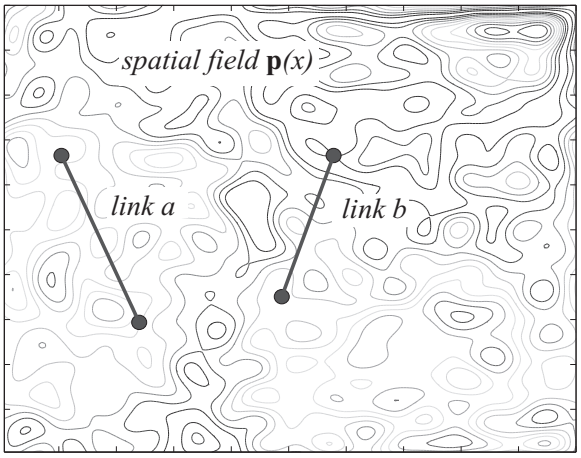

Fig. 5. A link pair in an underlying spatial loss field $p(\mathbf{x})$.

B. Shadowing Losses

We propose to model the shadowing on links $X_{m,n}$, for all pairs of nodes (m,n), as a function of the spatial loss field $p(\mathbf{x})$. The correlation between shadowing losses on many links derives from the fact that all links' shadowing values are described as a function of the one spatial loss field. Specifically, each link's shadowing loss $X_{m,n}$ is a weighted integral of the spatial loss field,

$$X_{m,n} \triangleq \frac{1}{\|\mathbf{x}_n-\mathbf{x}_m\|^{1/2}}\int_{\mathbf{x}_m}^{\mathbf{x}_n} p(\mathbf{x})d\mathbf{x}. \quad (9)$$

In short, (9) estimates the shadowing on an arbitrary link as a weighted line integral of the spatial loss field on which the link impinges. The units of $X_{m,n}$ are (dB); it is the shadowing loss caused by the link impinging on the spatial loss field $p(\mathbf{x})$.

A line integral along the path of the spatial loss field is an intuitive approximation for a path's loss, and has been used in many previous site-specific path loss models. In [32], the shadowing on an indoor-outdoor link at 5.85 GHz is modeled in a "partition-based model" as a sum of the losses caused by objects through which the straight line between the two nodes crosses. Site maps and floor plans are used to calculate the number of each kind of object for each link. The partition-based model reduces the standard deviation of model error to 2.6 dB, compared to a standard deviation of 8.0 dB using a purely distance-based path loss model. In [33], shadowing losses are also represented as a line integral for the purpose of extrapolating signal strength measurements beyond the points at which they have been measured. The model uses a land use and terrain map to derive a piece-wise constant loss field (with units of dB attenuation per unit distance). The total path loss on a link is equal to the large scale path loss of (1) plus a line integral of the loss field. The difference in our proposed model is that the loss field is not a piece-wise constant function, and is statistical, rather than determined by a map.

The normalization in (9) is both necessary to explain physical behavior of links and intuitively acceptable. Consider an example of two different links: a short link of 5 m; and a long link of 500 m. When an attenuating object (*e.g.*, vehicle) drives into the line of the short link, it attenuates the signal. In relative terms, when the same vehicle drives into the line of the long link, it typically attenuates the signal less strongly. This is because the relative loss of diffracting or scattering over or around the vehicle is less, typically, for the long link. This is why the loss in a link cannot simply be a sum of all attenuation caused in the line-of-sight path – it must be a weighted integral that downweights loss for longer links. The reason the weight must be proportional to $d^{-1/2}$ is that this function of d makes the variance of shadowing constant vs. d, which is required for the model to have Property I, as described and proven below.

In summary, relevant site-specific models suggest that a line integral is an appropriate model for shadowing caused by major obstructions on a link. Weighting is suggested to agree with the intuition that individual attenuating objects are not as important for links with longer path lengths. Next, we prove that (9) agrees with known properties of shadowing loss on a single link, and then show that it leads to positive covariances between shadowing losses on multiple links.

1) Single-Link Properties: The proposed model agrees with two important empirically-observed link shadowing properties:

Prop-I The variance of dB shadowing on a link is approximately constant with the path length [6],[7],[34].

Prop-II Shadow fading losses (in dB) are Gaussian.

The model in (9) can be seen to have Prop-II, since $X_{m,n}$ is a scaled integral of a Gaussian field. The proposed model has Prop-I when $\|\mathbf{x}_j - \mathbf{x}_i\| >> \delta$. We show this by considering $\text{Var}\left[X_a\right]$ for link $a = (i,j)$,

$$\text{Var}\left[X_a\right] = \frac{1}{\|\mathbf{x}_j - \mathbf{x}_i\|} \int_{\boldsymbol{\alpha}=\mathbf{x}_i}^{\mathbf{x}_j} \int_{\boldsymbol{\beta}=\mathbf{x}_i}^{\mathbf{x}_j} R_p(\|\boldsymbol{\beta} - \boldsymbol{\alpha}\|) d\boldsymbol{\alpha}^T d\boldsymbol{\beta}. \tag{10}$$

Using (7) as the model for spatial covariance, (10) is given by

$$\text{Var}\left[X_a\right] = \sigma_X^2 \left[1 + \frac{\delta}{\|\mathbf{x}_j - \mathbf{x}_i\|} e^{-\|\mathbf{x}_j - \mathbf{x}_i\|/\delta} - \frac{\delta}{\|\mathbf{x}_j - \mathbf{x}_i\|}\right], \tag{11}$$

and when $\|\mathbf{x}_j - \mathbf{x}_i\| >> \delta$,

$$\text{Var}\left[X_a\right] \approx \sigma_X^2. \tag{12}$$

2) Joint Link Properties: Consider two links $a = (i,j)$ and $b = (k,l)$, as shown in Fig. 5, with shadowing X_a and X_b, respectively. The covariance of X_a and X_b is,

$$\text{Cov}\left(X_a, X_b\right) = \frac{\sigma_X^2}{\delta d_{i,j}^{1/2} d_{k,l}^{1/2}} \int_{C_{i,j}} \int_{C_{k,l}} e^{-\frac{\|\boldsymbol{\beta} - \boldsymbol{\alpha}\|}{\delta}} d\boldsymbol{\alpha}^T d\boldsymbol{\beta}. \tag{13}$$

where $d_{i,j} = \|\mathbf{x}_i - \mathbf{x}_j\|$ and, $C_{m,n}$ is the line between points $\mathbf{x}_m$ and $\mathbf{x}_n$.

The solution to (13) is tedious to derive analytically. We use numerical integration to compute the value of ρ_{X_a,X_b}. Matlab calculation code for this purpose is available on the authors' website [35].

C. Total Fading Model

Since shadowing loss $X_{i,j}$ is only one part of the total fading loss $Z_{i,j} = X_{i,j} + Y_{i,j}$, we must also consider the model for non-shadowing losses $Y_{i,j}$. We note that shadow fading and non-shadow fading are caused by different physical phenomenon, and thus $X_{i,j}$ and $Y_{i,j}$ can be considered as independent. The variance of total fading, $\text{Var}\left[Z_{i,j}\right]$, is thus,

$$\sigma_{dB}^2 \triangleq \text{Var}\left[Z_{i,j}\right] = \text{Var}\left[X_{i,j} + Y_{i,j}\right] = \text{Var}\left[X_{i,j}\right] + \text{Var}\left[Y_{i,j}\right]. \tag{14}$$

Non-shadow fading is predominantly composed of narrow-band or small-scale fading, which can be well-approximated to have zero correlation over distances greater than a few wavelengths. Since multi-hop networks typically have sensors spaced more than a few wavelengths apart, $\{Y_{i,j}\}_{(i,j)}$ are considered independent across link pairs in this paper. If multi-hop networks are designed with antennas spaced closer than a few wavelengths, this independence assumption could easily be replaced with a valid correlated small-scale fading model.

D. Analysis Using Proposed Model

In this section, we show how the model may be applied in simulation or analysis. In short, the vector of all link path losses $\{Z_{i,j}\}_{ij}$ in a deployed network can be modeled as a joint Gaussian random variables with zero mean and a given covariance matrix. Specifically, define $\mathbf{z} = [Z_{i_1,j_1}, \ldots, Z_{i_N,j_N}]$, where $(i_1,j_1), \ldots, (i_N,j_N)$ is a list of unique links in the deployed network and N is the total number of links in the deployed network. According to the model, the covariance matrix of $\mathbf{z}$ is given by,

$$C_Z(\boldsymbol{\theta}) = C_X(\boldsymbol{\theta}) + \mathbb{I}_N \sigma_Y^2, \tag{15}$$

where $\mathbb{I}_N$ is the $N \times N$ identity matrix, σ_Y^2 is the variance of non-shadow fading, *i.e.*, $\sigma_Y^2 = \sigma_{dB}^2 - \sigma_X^2$, and

$$C_X(\boldsymbol{\theta}) = \left[\left[\text{Cov}\left(X_{i_k,j_k}, X_{i_l,j_l}\right)\right]\right]_{k,l}, \tag{16}$$

where $\text{Cov}\left(X_{i_k,j_k}, X_{i_l,j_l}\right)$ is defined for arbitrary links in (13) as a function of the parameters δ and σ_X^2. Note that the total fading values $\{Z_{i,j}\}$ are zero mean. Since we have assumed $\{Z_{i,j}\}$ to be multi-variate Gaussian, the mean and covariance matrix completely determine the distribution as a function of $\boldsymbol{\theta}$.

In simulation, Gaussian random vectors with an arbitrary covariance matrix are generated by first generating i.i.d. Gaussian vectors and multiplying them by the square root of the covariance matrix. In analysis, Gaussian models are often convenient compared to more complicated distributional models. Analysis in [27] used the given joint path loss model to find an analytical lower bound for sensor localization variance. In this paper, we present a mix of analysis and simulation results in Section VI.

V. Experimental Validation

A statistical joint path loss model must be validated by measurements of the joint path loss across many deployed networks. In this section, we present two measurement campaigns, in a controlled indoor environment and in an uncontrolled outdoor environment, at 900 and 2400 MHz. We

present the methods which we apply to the measurements to validate the proposed model, quantify link correlations, and estimate model parameters. The first part of this section describes the measurement campaigns, including descriptions of the environment, equipment, and measurement protocol. In the second part of this section, we present the statistical analysis of measurement data, including the estimation of the model parameters, the space constant δ and the variance of shadowing σ_X^2.

A. Measurement Campaign Overview

For validation of the proposed joint path loss model, we have carried out two measurement campaigns. Each measured several realizations of wireless sensor networks, each network with several nodes and many measured links. In each network, the received signal strengths of all pair-wise links are measured and the results saved. In addition, in each deployment, the actual positions of all nodes are carefully determined and recorded. We believe that the time complexity of carrying out such measurements has in the past been a barrier to the study of link shadowing correlations in multi-hop wireless networks.

The two measurement campaigns presented in this section are carried out in different manners in order to achieve particular purposes. These purposes are:

1) *Controlled Measurement Campaign*: Study many realizations of networks with an identical node geometry in a controlled, repeatable experimental setup. Many identical-geometry measurements allow us to experimentally characterize correlation for particular geometries of pairs of links.
2) *Field Deployment Measurement Campaign*: Demonstrate shadowing correlations between links in natural, uncontrolled environments.

Campaign (1.) measured fifteen network realizations, each with sixteen nodes; campaign (2.) measured six network realizations, each with 16-19 nodes. In total, signal strength measurements on over 2700 different links were made and recorded. Campaigns (1.) and (2.) operated in the 902-928 MHz, and 2400-2483 MHz, U.S. ISM bands, respectively. For each link, measurements were repeated at 16 different center frequencies within the band of operation and repeated over time in order to average out narrow-band fading effects and changes due to motion in the environments. The large set of data allows us to validate the claim that shadowing losses are correlated between links, and to determine the parameters of the proposed joint path loss model.

B. Controlled Measurement Campaign

The first measurement campaign is designed to provide a random environment but yet provide a repeatable experimental procedure. In this campaign, we leave sixteen nodes deployed in a grid geometry in a classroom and then, before each new measurement experiment, randomly vary the positions of obstructions within the room. Fifteen different random obstruction arrangements are created, corresponding to fifteen realizations of a random environment.

This controlled experimental setup allows us to test many wireless networks with the identical node geometry, without the difficulty of finding that many different places which would allow nodes to be positioned in exactly the same geometry. Further, the experiment could readily be repeated by other researchers who want to measure link shadowing correlations, without access to the identical building used in this campaign.

The controlled measurement campaign begins by deploying nodes in an empty classroom in the Merrill Engineering Building at the University of Utah, in a 4x4 square grid of node locations with 4 ft (1.22 m) spacing between neighboring nodes. Nodes are placed on the floor at each grid point. Within this deployment area, we generate a *random environment* by randomly placing 10 cardboard boxes wrapped with aluminum foil. Foil-wrapped cardboard boxes represent metal obstacles which might be present in office environments. A Matlab script generates the random location of these boxes within the area of deployment.

This first experiment uses Crossbow Mica2 wireless sensor devices [36], which operate in the 900-928 MHz band. Sensors are programmed with a TinyOS 1.x/NesC program to collect a large number of pairwise received signal strength (RSS) measurements. Sensors use a TDMA-based MAC protocol in which each wireless sensor broadcasts during an assigned slot to avoid interference with other sensors. Each broadcast contains the RSS values the sensor has measured during the most recent measurement period. One node overhears all broadcasts and logs the pairwise measurements over time. Nodes serially change frequency to 14 different center frequencies in the frequency band (902-928 MHz). The nodes are synchronized and programmed to frequency hop and measure RSS at each frequency. NesC code can be downloaded from the authors website [35].

In summary, in this measurement campaign, we randomly change the environment while keeping a constant grid geometry of the network nodes. We will show that the large number of networks with an identical geometry allow the study of particular geometries of pairs of links to show particular cases of how geometries affect link shadowing correlation.

C. Field Deployment Measurement Campaign

The field deployment measurement campaign is carried out in two natural areas near Salt Lake City, Utah. These areas are Red Butte Canyon, an arid canyon area in the foothills of the Wasatch Mountain range (about 5,200 ft elevation), and Albion Basin, a high mountain valley at the top of Little Cottonwood Canyon, at an elevation of 10,000 ft. Measurements were conducted in Summer, and at the low elevation, the vegetation consists of dry grasses, sage brush, and scrub oak. At the high elevations, the vegetation consists of many trees, including maples, pines, and willows, with a dense ground cover of flowering plants and shrubs. In both environments, terrain varies rapidly, with variation in ground height from 5-20 ft within a deployment area. We measure two network deployments in Red Butte Canyon and four deployments in Albion Basin.

In this campaign, measurements are carried out using a network of nineteen Crossbow TelosB wireless sensor devices.

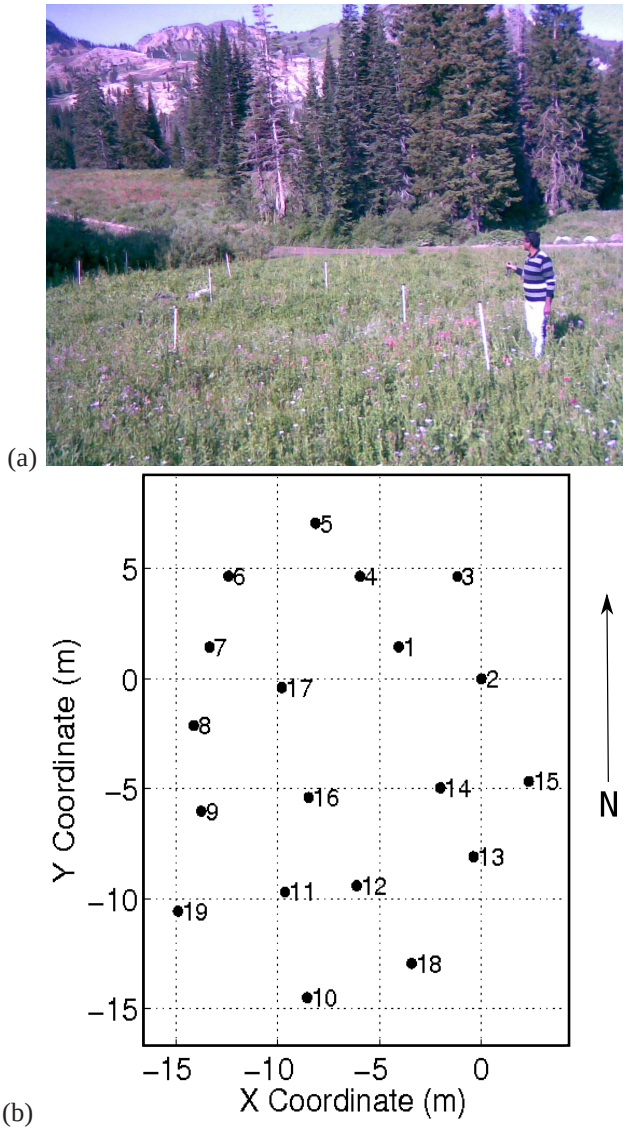

Fig. 6. Figure (a) shows one realization of the network deployment at Albion Basin. The map constructed by such deployment of wireless sensors is shown in (b).

These are 802.15.4-compliant radios which operate 2.4-2.48 GHz ISM band. Wireless sensors are kept at a height of 1 m using stands. After deployment, the coordinate of each sensor is carefully determined using a measuring tape and a compass. Such positioning measurements are overdetermined so that we can verify that sensor positions are determined accurately. The network geometry is random, depending on where it is possible to position the sensors within the varying terrain and vegetation. The sizes of network deployments range from 400 m^2 to 1800 m^2. A map of one such network deployment is shown in Fig. 6.

In this campaign, deployments are significantly larger in area than in the indoor campaign. Due to the range and the varying terrain and vegetation, we do not have fully connected networks. In particular, one eavesdropping node cannot reliably overhear all packet traffic from all nodes in the network. In these deployments, we use a protocol which forwards all measured data (over possibly multiple hops) to a root node for data collection purposes.

We accomplish data collection using a protocol which builds upon the TinyOS 2.0 "Collection Tree" protocol. Collection Tree creates a tree from the root node to each sensor based on a link quality indicator (LQI) metric [37]. First, deployed TelosB nodes perform a number of RSS measurements at a single frequency, and then average them. Next, all average RSS values are routed to the root node via Collection Tree and recorded on a laptop. Similar to the first campaign, nodes change center frequencies within the band of operation, and synchronize such that all nodes are transmitting and receiving on the same center frequency at the same time.

When one network deployment is finished measuring across all center frequencies and we have verified that full data has been recorded, we pick up the network, move up or down the canyon, redeploy in a new area, and re-determine sensor positions. The geometry of each network is unique because the area in which it is placed introduces unique limitations on where nodes can be positioned.

In summary, the field deployment measurement campaign allows the deployment of relatively large networks in random natural environments, each with a different network geometry, and each in a naturally determined positioning of obstructions.

D. Statistical Analysis

With the large quantity of measured data, we hope to accomplish two main goals:

1) *Estimate* the parameters of the model in the two measurement campaigns, and
2) *Verify* that the shadowing on pairs of link are correlated and that the proposed model agrees with the measured correlations.

This subsection presents the analysis to accomplish both goals. Model parameter estimation includes:

1) *Large-scale path loss parameters*: n_p and $P_T - \Pi_0$ of (2), and
2) *Correlated shadowing parameters*, δ and σ_X^2 of (7).

Large-scale analysis determines the average path loss vs. distance; shadowing and other types of fading are what remain after large-scale path loss is removed. Thus large-scale path loss parameters are estimated first.

1) Estimation of Large-Scale Path Loss Parameters: For each realization of network, $m \in \{1, \ldots, M\}$, where M is the total number of network realizations in each measurement campaign, the frequency-averaged RSS (in dB) between two nodes i and j, $P_{i,j}^{(m)}$, is represented by a distance-dependent path loss model (2), (3)

$$P_{i,j}^{(m)} = P_{T_j} - \Pi_0 - 10 n_p \log \frac{d_{i,j}}{\Delta_0} - X_{i,j}^{(m)} - Y_{i,j}^{(m)}, \quad (17)$$

where $X_{i,j}^{(m)}$ is the shadow fading, $Y_{i,j}^{(m)}$ is the non-shadow fading, for the mth realization of link (i, j), which has length $d_{i,j}$. Because $Y_{i,j}$ is an average of measurements across many different frequencies, we argue that it may be approximated as Gaussian (in dB), regardless of the underlying frequency-selective fading mechanism (*e.g.*, Rayleigh or Ricean). Shadow

fading is typically modeled as Gaussian (in dB) [34], so we expect the total fading $Z_{i,j}^{(m)} = X_{i,j}^{(m)} + Y_{i,j}^{(m)}$ (in dB) to be Gaussian.

The model of (17) is a linear model for received power as a function of the log of the path length. Thus we use linear regression to estimate the "point" and "slope" of the linear model, which are $(P_T - \Pi_0)$ and n_p. In our analysis, we use $\Delta_0 = 1$ m. All nodes are set to the same transmit power and we monitor for equal battery voltages, so we expect transmit power P_T to be approximately constant across nodes.

2) Estimation of Correlated Shadowing Parameters: Once the large scale path loss model parameters n_p and $(P_T - \Pi_0)$ are determined, the next step is to estimate the parameters of correlated shadowing model introduced in Section IV. We define the parameter vector to be estimated as $\boldsymbol{\theta}$, where $\boldsymbol{\theta} = \left[\delta, \frac{\sigma_X^2}{\sigma_{dB}^2}\right]^T$.

From the residues of the large-scale path loss linear regression, the total fading loss $Z_{i,j}^{(m)}$ for each link (i,j) and the overall variance of $Z_{i,j}^{(m)}$, *i.e.*, σ_{dB}^2, are determined. Then, we define $\mathbf{z}^{(m)} = \left[Z_{i_1,j_1}^{(m)}, \ldots, Z_{i_N,j_N}^{(m)}\right]$, where $(i_1,j_1), \ldots, (i_N,j_N)$ is a list of unique measured links in the network and N is the total number of links in the deployed network. According to the model, $\mathbf{z}^{(m)}$ is zero-mean with covariance matrix given by (15).

We use maximum likelihood estimation for estimating parameter $\boldsymbol{\theta}$. In other words, we find $\boldsymbol{\theta}_{MLE}$ which maximizes the conditional likelihood function given by (18),

$$\begin{aligned} f(\mathbf{z}|\boldsymbol{\theta}) &= \prod_m f(\mathbf{z}^{(m)}|\boldsymbol{\theta}) \\ &= \prod_m \frac{1}{(2\pi)^{N/2}|C_Z(\boldsymbol{\theta})|^{1/2}} \exp\left[-\frac{1}{2}\mathbf{z}^{(m)T} C_Z^{-1}(\boldsymbol{\theta})\mathbf{z}^{(m)}\right], \end{aligned} \tag{18}$$

where $|\cdot|$ denotes the determinant of the matrix and $\cdot^T$ denotes the transpose. Equivalently, $\boldsymbol{\theta}_{MLE}$ can be found by finding the maximum of the log likelihood function $l(\mathbf{z}|\boldsymbol{\theta}) = \log f(\mathbf{z}|\boldsymbol{\theta})$,

$$l(\mathbf{z}|\boldsymbol{\theta}) = \sum_m \left[-k - \frac{1}{2}|C_Z(\boldsymbol{\theta})| - \frac{1}{2}\mathbf{z}^{(m)T} C_Z^{-1}(\boldsymbol{\theta})\mathbf{z}^{(m)}\right]. \tag{19}$$

where $k = \frac{N}{2}\log(2\pi)$ is a constant.

For lack of an analytical solution to the maximization of (19), we use a brute force approach. The log likelihood $l(\mathbf{z}|\boldsymbol{\theta})$ is computed for a wide range of $\boldsymbol{\theta}$, specifically, $\delta \in [0.1, 0.9]$ in increments of 0.01, and $\sigma_X^2/\sigma_{dB}^2 \in [0.1, \ldots, 0.9]$ in increments of 0.01. The value of $\boldsymbol{\theta}_{MLE}$ for the controlled measurement campaign is found to be $\boldsymbol{\theta}_{MLE} = [0.30, 0.41]^T$, and for the field deployment measurement campaign, $\boldsymbol{\theta}_{MLE} = [0.57, 0.55]^T$.

3) Discussion: The first parameter δ of the proposed model is the distance constant in the correlated random spatial loss field $p(\mathbf{x})$. It describes the separation at which the correlation between two points in that spatial loss field have correlation coefficient of e^{-1}. Loosely, we can describe it as a measure of the 'size' of attenuating obstructions in the environment. Comparing the controlled and field deployment measurement campaigns, the average sizes of obstructions in the indoor controlled campaign (boxes) are smaller than in the field deployment campaign (terrain and vegetation). Thus, we would expect the parameter δ to be greater in field deployment campaign compared to the controlled campaign, and in fact, the δ parameter in the field deployment campaign is almost double.

The second parameter σ_X^2/σ_{dB}^2 represents the relative contribution of shadowing, $X_{i,j}$, to total fading, $Z_{i,j}$. It is a function of the type of environment. Indoor environments have a higher angular spread of arriving multipath, due to more significant reflections, compared to the outdoor environments, so narrowband fading will be more significant. The analysis from the measurement campaigns concludes that for the outdoor field deployment measurement campaign, the contribution of shadowing to total fading is 55%, compared to 41% in the indoor controlled measurement campaign.

E. Verification

The repeated geometries in the controlled measurement campaign allow us to look at specific geometries of links in more detail. First, we use the measurements to verify that the shadowing on many realizations of specific *link pair geometries* do in fact show statistically significant correlations. Second, we show that the proposed correlated link shadowing model does suggest correlation coefficients similar to those estimated from measurements.

We refer to a *link pair geometry* as any pair of links with the same coordinates of endpoints within a translation and rotation. For example, consider link pair geometry #1 in Table I. Any two links which have a common endpoint, extend in the same direction from that endpoint, and have one link of length one unit and the other link of length two units, have link pair geometry #1. Many such link pair geometries are shown in Table I. Since we have fifteen realizations of identical-geometry networks, and many pairs of links within each network which have an identical link pair geometry, we verify from a large set of realizations that shadowing values are correlated. Let $\{Z_{a_i}, Z_{b_i}\}$ be a set of measured total fading pairs, where $(a_1,b_1), \ldots, (a_P,b_P)$ are the pairs of measured links which have a particular link pair geometry. Then we compute the experimental correlation coefficient $\hat{\rho}$ between $\{Z_{a_i}\}$ and $\{Z_{b_i}\}$.

Using a statistical test for correlation [38, pp. 427-431], we test between the two hypotheses:

$$\begin{aligned} H_0 &: \ Z_a \text{ and } Z_b \text{ have } \rho = 0, \\ H_1 &: \ Z_a \text{ and } Z_b \text{ have } \rho \neq 0. \end{aligned}$$

In hypothesis testing, H_0 is the null hypothesis. We assume H_0 is true, unless experimental evidence shows beyond a reasonable doubt that H_0 is not true. If $\rho = 0$, this does not mean that every link pair geometry would measure $\hat{\rho} = 0$. The measurements are random, and in fact, the event $\{\hat{\rho} = 0\}$ has probability zero. Instead, the hypothesis test says that when the measured $|\hat{\rho}|$ exceeds a particular threshold (which is a function of the number of measurements and desired probability of false alarm), it means that H_0 is very unlikely to have been true. The threshold is determined by the desired

	Geometry	Correlation ρ			Geometry	Correlation ρ	
		Measured	Prop. Model			Measured	Prop. Model
1		0.33***	0.31	**14**		-0.04	0.09
2		0.21***	0.25	**15**		0.12***	0.18
3		0.23***	0.35	**16**		0.08*	0.12
4	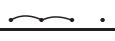	0.05	0.06	**17**		0.12***	0.18
5		0.17***	0.29	**18**		0.03	0.17
6	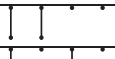	-0.05	0.01	**19**	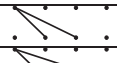	0.21***	0.22
7	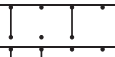	-0.01	0.00	**20**	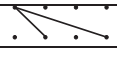	-0.02	0.13
8	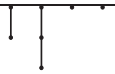	-0.10**	0.01	**21**	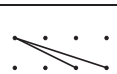	0.23***	0.26
9		-0.03	0.09	**22**		0.00	0.08
10		0.04*	0.15	**23**	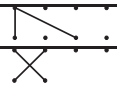	0.08**	0.22
11		0.14***	0.15	**24**		0.12	0.23
12		0.17***	0.15	**25**		0.08	0.00
13	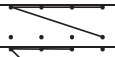	0.05	0.11	**26**		0.03	0.04

p-value, *i.e.*, P[getting measured $\rho | H_0$]

*** $p < 0.005$ ** $p < 0.01$ * $p < 0.05$

TABLE I
LINK GEOMETRY AND CORRELATION COEFFICIENTS (OBSERVED, PROPOSED MODEL)

probability of false alarm, p, so that only in rare cases would the test decide H_1 if H_0 was actually true. We report in Table I the cases for which the test decides H_1 given three different false alarm rates p of 0.05, 0.01, and 0.005. In Table I tests which are statistically significant at these three false alarm rates are denoted with a *, **, and ***, respectively. There are ten link geometries shown which have a p-value of less than 0.005; it is extremely unlikely that fading on these pairs of links is uncorrelated. We note that link pair geometries which have greater "overlap" or "proximity" have higher correlation in shadow fading. This is intuitive because a greater overlap means a larger similarity in the environment through which the two links pass.

The proposed model is shown to have positive shadowing correlations between link pairs which do show significant shadow fading correlations. Table I lists the correlation coefficient computed from the correlated shadowing model (using the parameters $\delta = 0.30$ and $\sigma_X^2/\sigma_{dB}^2 = 0.41$ estimated from the controlled measurement campaign). The model-based correlation value ρ is not equal to the experimental correlation estimate $\hat{\rho}$, but is often very close, and generally is high when the measured $\hat{\rho}$ is high. Measurements and model particularly agree well when the number of measurements for the particular link pair geometry is high; link pair geometry #1 is repeated many (32) times in each measured network, many more times than link pair geometry #5 (which is repeated 8 times in each measured network).

Further, we expect that (1.) since each measurement is random, the $\hat{\rho}$ computed from measurements is also random, and (2.) that our proposed model does not explain all facets of the environment which cause correlated shadowing. In particular, we note that a link pair geometry #8 records a statistically significant negative correlation coefficient, but that our proposed model only predicts non-negative shadowing correlations. Studying mechanisms which cause negative link shadowing correlations is a topic of future research.

In summary, the results from the controlled measurement experiment provide a large set of measurements from pairs of links with identical relative geometries. These data show that particular geometries of proximate link pairs show statistically significant correlation, in other words, it is highly unlikely that link pairs of these geometries have uncorrelated shadow fading. We can quantify these correlations and the proposed method provides a statistical model to explain these correlations.

VI. APPLICATION OF JOINT MODEL

Correlated shadowing is important because it has a major impact in mesh, ad hoc, and sensor networks. It is something experienced in deployed multi-hop networks which is not, in state-of-the-art statistical channel models, represented in simulation or analysis of such networks. As discussed in Section I-B, existing statistical and deterministic path loss models have been applied in networking research. We show in this section that the impact of correlated shadowing on end-to-end performance statistics in deployed multi-hop networks is significant. In this section, we give two examples of the differences between performance results when comparing the output of an i.i.d. shadowing model with the output of a correlated shadowing model. In general, for arbitrary larger deployments, we expect the effects of correlated shadowing to

Measurement Campaign	Controlled	Field Deployment
Environment	Indoor classroom	Outdoor canyon
# Network Realizations	15	6
# Nodes	16	16-19
Freq. Band	900-928 MHz	2.4-2.48 GHz
Est. δ	0.30	0.57
Est. σ_X^2/σ_{dB}^2	0.41	0.55

TABLE II
SUMMARY OF TWO MEASUREMENT CAMPAIGNS

be even more significant, but we analyze two simple networks in this section for clarity of explanation.

To simplify the analysis we assume,

1) Packets are received if and only if the received power is greater than a receiver threshold γ, and
2) No packets are lost due to interference.

These assumptions do not limit the results in this section. In fact, performance in interference is also affected by joint path losses between the interfering transmitter and the two communicating nodes, and thus is also impacted by correlated shadowing.

We denote the *normalized received power above the threshold* for a link (m,n), as $\beta_{m,n}$,

$$\beta_{m,n} = \frac{P_{m,n} - \gamma}{\sigma_{dB}} \tag{20}$$

where γ is the threshold received power, $P_{m,n}$ is received power given in (2) and σ_{dB} is the standard deviation of total fading in the network. Link (m,n), by assumption, is connected if and only if $\beta_{m,n} > 0$. An important system parameter is the expected value of $\beta_{m,n}$,

$$\bar{\beta}_{m,n} \triangleq E\left[\beta_{m,n}\right] = \frac{\bar{P}(d_{m,n}) - \gamma}{\sigma_{dB}} \tag{21}$$

where $\bar{P}(d_{m,n})$ is given in (1). Intuitively, $\bar{\beta}_{m,n}$ is the number of standard deviations, σ_{dB}, of link margin we have in link (m,n). If we design the multi-hop network with higher $\bar{\beta}_{m,n}$, we will have a higher robustness to the actual fading in the environment of deployment. For example, one could set the inter-node distance to ensure that $\bar{\beta}_{m,n} = 2$, and then link (m,n) would only be disconnected if total fading loss was two standard deviations more than its mean.

A. A Three Node Multi-Hop Path

Consider the simple multi-hop path shown in Fig. 7(a), which represents a part of a typical multi-hop network. In this example, $||\mathbf{x}_i - \mathbf{x}_j|| = ||\mathbf{x}_j - \mathbf{x}_k||$. For node i to transmit information to node k, the message packet can take two routes. One is the direct link (i,k) and the other is a two hop path through a relay node j, *i.e.*, through link (i,j) and then through link (j,k). If for our particular deployment, the link (i,k) fails due to high shadowing, there is a chance that the message can still arrive via links (i,j) and (j,k). This section shows that this 'link diversity' method is not as robust as would be predicted assuming independent link shadowing.

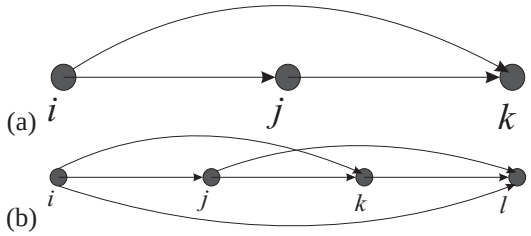

Fig. 7. Example multi-hop networks of (a) three and (b) four nodes.

We define two events relating to the connectedness of links,

$$\begin{aligned}\mathcal{A} &= \{\text{Link } (i,k) \text{ is connected}\} = \{\beta_{i,k} > 0\} \\ \mathcal{B} &= \{\text{Link } (i,j) \text{ and link } (j,k) \text{ are both connected}\} \\ &= \{\beta_{i,j} > 0\} \cap \{\beta_{j,k} > 0\}.\end{aligned} \tag{22}$$

Then $\mathcal{A} \cup \mathcal{B}$ is the event that two nodes i and k can communicate, either directly or through an intermediate node j. The probability that node i and k cannot communicate is the *probability of path failure*,

$$1 - P\left[\mathcal{A} \cup \mathcal{B}\right] = 1 - \left(P\left[\mathcal{A}\right] + P\left[\mathcal{B}\right] - P\left[\mathcal{A} \cap \mathcal{B}\right]\right). \tag{23}$$

From (21) and (1), the relationship between $\bar{\beta}_{i,j}$, $\bar{\beta}_{j,k}$ and $\bar{\beta}_{i,k}$ for the simple three-node network is,

$$\bar{\beta}_{i,j} = \bar{\beta}_{j,k}; \quad \text{and} \quad \bar{\beta}_{i,k} = \bar{\beta}_{i,j} - \kappa. \tag{24}$$

where $\kappa = \frac{10 n_p \log_{10} 2}{\sigma_{dB}}$. According to the definition (22), the probability of event $\mathcal{A}$ is,

$$P\left[\mathcal{A}\right] = P\left[\{\beta_{i,k} > 0\}\right] = \mathrm{Q}\left(-\bar{\beta}_{i,k}\right) = 1 - \mathrm{Q}\left(\bar{\beta}_{i,j} - \kappa\right) \tag{25}$$

where $\mathrm{Q}(\cdot)$ is the complementary CDF of a standard Normal random variable.

1) Case of i.i.d. Shadowing: Under the assumption that the shadowing across links in a network is i.i.d., the probability of event $\mathcal{B}$ is

$$P\left[\mathcal{B}\right] = P\left[\{\beta_{i,j} > 0\} \cap \{\beta_{j,k} > 0\}\right] = (1 - \mathrm{Q}\left(\bar{\beta}_{i,j}\right))^2. \tag{26}$$

From (26) and (23), the probability of path failure is

$$1 - P\left[\mathcal{A} \cup \mathcal{B}\right] = \mathrm{Q}\left(\bar{\beta}_{i,j} - \kappa\right)\mathrm{Q}\left(\bar{\beta}_{i,j}\right)[2 - \mathrm{Q}\left(\bar{\beta}_{i,j}\right)]. \tag{27}$$

2) Case of Correlated Shadowing: From the correlation values reported in Table I, we know that links (i,j) and (j,k) of Fig. 7(a) are nearly uncorrelated. Thus, the probability for event $\mathcal{B}$ is approximately the same as in i.i.d. case. The probability $P\left[\mathcal{A} \cap \mathcal{B}\right]$ for the case of correlated shadowing is derived in the appendix. Combining the results from appendix,

(23), (24) and (26), the probability of path failure when shadowing on links is correlated is

$$1 - P\left[\mathcal{A} \cup \mathcal{B}\right] = \mathrm{Q}\left(\bar{\beta}_{i,j} - \kappa\right) - \left(1 - \mathrm{Q}\left(\bar{\beta}_{i,j}\right)\right)^2 + P\left[\mathcal{A} \cap \mathcal{B}\right], \tag{28}$$

where

$$P\left[\mathcal{A} \cap \mathcal{B}\right] = \int_{\beta_{i,k}>0} \left[\mathrm{Q}\left(\frac{-\mu_1}{\sqrt{1-\rho^2_{X_{i,j},X_{i,k}}}}\right)\right]^2 e^{-\frac{(\beta_{i,k}-\bar{\beta}_{i,j}+\kappa)^2}{2}} d\beta_{i,k},$$

and, $\mu_1 = \bar{\beta}_{i,j} + (\beta_{i,k} - \bar{\beta}_{i,j} + \kappa)\rho_{X_{i,j},X_{i,k}}$.

B. A Four Node Multi-Hop Network

Next, consider the four node link shown in Fig. 7(b). For this linear deployment we assume $||\mathbf{x}_i - \mathbf{x}_j|| = ||\mathbf{x}_j - \mathbf{x}_k|| = ||\mathbf{x}_k - \mathbf{x}_l||$. For node i to communicate with node l, the message packet can be routed in four different ways, as shown in Fig. 7(b).

An analytical expression for the probability of path failure is tedious, so instead we simulate the network shown in Fig. 7(b) in both the cases of correlated and i.i.d. link shadowing. We take 10^5 samples of the normalized received powers under both correlated shadowing and i.i.d shadowing models. We then determine from the result the probability of path failure, *i.e.*, that there exists *no* connected path from node i to node l.

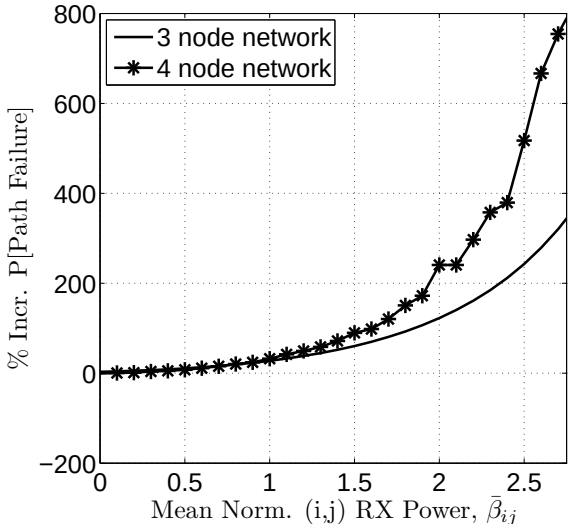

Fig. 8. The percentage increase in P [link failure] for correlated, vs. i.i.d. shadowing, for 3 and 4 node multi-hop network examples, as a function of $\bar{\beta}_{i,j}$.

C. Discussion

We compare the probability of path failure between node i and node k for both the cases of i.i.d. and correlated link shadowing in Fig. 8. The analysis shows that when a multi-hop network is designed for $\bar{\beta}_{i,j} = 2, \forall(i,j)$, then the probability of path failure is 120% greater in correlated shadowing as compared to i.i.d. shadowing. Increasing the reliability of the network by designing it for higher $\bar{\beta}_{i,j}$ only increases the disconnect between the two models. It is only when we design the network for very unreliable links (*e.g.*, $\bar{\beta}_{i,j} = 0$, for which link (i,j) is connected half of the time) that the models have a similar result. Path connectivity is much more likely under the i.i.d. model than under the realistic correlated link shadowing model.

The four-node example shows that as paths become longer, it becomes increasingly important to consider correlated link shadowing. While the 3-node network had a 120% increase in probability of path failure, the 4-node network showed a 200% increase in the same probability. While Fig. 8 show the results up to $\bar{\beta}_{i,j} = 2.5$, higher values correspond to higher reliability links, and reliable networks will be designed with even higher link margins. When networks are designed for high reliability, the effects of ignoring link shadowing correlations are dramatic.

VII. Conclusion

We presented the need for statistical path loss models for multi-hop (sensor, ad hoc, and mesh) networks which model the correlation in shadow fading between proximate links. We discussed why existing correlated shadowing models do not apply to arbitrary geometries of links like those which exist in multi-hop networks. We present a new statistical joint path loss model that relates the shadow fading on different links in a multi-hop network to the random underlying spatial loss field. Two measurement campaigns are conducted to measure path losses in indoor and outdoor environments and in two different bands, 900 and 2400 MHz. The data sets demonstrate statistically significant shadowing correlations among particular geometries of link pairs and show that correlated shadowing can be measured in a repeatable experimental setup as well as in natural outdoor environmental sensor network deployments. Model parameters are given for these two campaigns. Finally, we analyze path connectivity statistics in simple multi-hop networks to show the importance of the consideration of shadowing correlation in reliable network design. Using the i.i.d. shadowing model, the probability of end-to-end path failure is underestimated by a factor of two or more.

Future work will test other ensembles of deployments in a wider variety of environments. We are working towards implementations of the simulation model for standard networking simulation environments such as `ns-2`. The effects of correlated shadowing will have impact on higher layer networking protocols and algorithms, and in interference and multiple-access control, and future work will quantify these effects.

VIII. Acknowledgements

The authors wish to thank Jessica Croft for her help with the field deployment measurement campaign.

References

[1] H. Lee, A. Cerpa, and P. Levis, "Improving wireless simulation through noise modeling," in *Information Processing in Sensor Networks (IPSN'07)*, April 2007.

[2] C. Newport, D. Kotz, Y. Yuan, R. S. Gray, J. Liu, and C. Elliott, "Experimental evaluation of wireless simulation assumptions," *SIMULATION: Transactions of The Society for Modeling and Simulation International*, vol. 83, no. 9, pp. 643–661, September 2007.

[3] S. Seidel and T. Rappaport, "Site-specific propagation prediction for wireless in-building personal communication system design," *IEEE Trans. Vehicular Technology*, vol. 43, no. 4, pp. 879–891, Nov. 1994.

[4] M. Hassan-Ali and K. Pahlavan, "A new statistical model for site-specific indoor radio propagationprediction based on geometric optics and geometric probability," *IEEE Trans. Wireless Communications*, vol. 1, no. 1, pp. 112–124, Jan. 2002.

[5] G. Marconi, "Wireless telegraphy," *Journal of the IEE*, vol. 28, pp. 273–315, 1899.

[6] H. Hashemi, "The indoor radio propagation channel," *Proccedings of the IEEE*, vol. 81, no. 7, pp. 943–968, july 1993.

[7] T. Rappaport, *Wireless Communication: Principles and Practice*, 2nd ed. Printice Hall, 1996.

[8] H. Bertoni, *Radio Propagation for Modern Wireless Systems*. Prentice Hall Professional Technical Reference, 1999.

[9] G. D. Durgin, *Space-Time Wireless Channel*. Prentice Hall Communication Engineering and Emerging Technologies Series, 2004.

[10] C. Bettstetter and C. Hartmann, "Connectivity of wireless multihop networks in a shadow fading environment," *Wirel. Netw.*, vol. 11, no. 5, pp. 571–579, 2005.

[11] R. Hekmat and P. V. Mieghem, "Connectivity in wireless ad-hoc networks with a log-normal radio model," *Mob. Netw. Appl.*, vol. 11, no. 3, pp. 351–360, 2006.

[12] D. Kotz, C. Newport, and C. Elliott, "The mistaken axioms of wireless-network research," Dept. of Computer Science, Dartmouth College, Tech. Rep. TR2003-467, July 2003. [Online]. Available: http://www.cs.dartmouth.edu/reports/abstracts/TR2002-467/

[13] A. A. Saleh and R. A. Valenzuela, "A statistical model for indoor multipath propagation," *IEEE J. Sel. Areas in Communications*, vol. 5, pp. 128–137, Feb. 1987.

[14] G. Malmgren, "On the performance of single frequency networks in correlated shadow fading," *IEEE Trans. Broadcasting*, vol. 43, no. 2, pp. 155–165, June 1997.

[15] K. S. Butterworth, K. W. Sowerby, and A. G. Williamson, "Base station placement for in-building mobile communication systems to yield high capacity and efficiency," *IEEE Trans. Communications*, vol. 48, no. 4, pp. 658–669, April 2000.

[16] T. Klingenbrunn and P. Mogensen, "Modelling cross-correlated shadowing in network simulations," in *IEEE VTC 1999*, vol. 3, Sept. 1999, pp. 1407–1411.

[17] J. Zhang and V. Aalo, "Effect of macrodiversity on average-error probabilities in a Rician fading channel with correlated lognormal shadowing," *IEEE Trans. Communications*, vol. 49, no. 1, pp. 14–18, Jan. 2001.

[18] A. Safak and R. Prasad, "Effects of correlated shadowing signals on channel reuse in mobile radio systems," *IEEE Trans. Vehicular Technology*, vol. 40, no. 4, pp. 708 – 713, Nov. 1991.

[19] M. Gudmundson, "Correlation model for shadow fading in mobile radio systems," *IEEE Elecronics Letters*, vol. 27, no. 23, pp. 2145–2146, November 1991.

[20] Z. Wang, E. K. Tameh, and A. Nix, "Simulating correlated shadowing in mobile multihop relay/ad-hoc networks," IEEE 802.16 Broadband Wireless Access Working Group, Tech. Rep. IEEE C802.16j-06/060, July 2006.

[21] N. Patwari, Y. Wang, and R. O'Dea, "The importance of the multipoint-to-multipoint indoor radio channel in ad-hoc networks," *IEEE Wireless Communication and Networking Conference (WCNC), Orlando FL*, March 2002.

[22] R. L. Moses, D. Krishnamurthy, and R. Patterson, "A self-localization method for wireless sensor networks," *EURASIP Journal on Applied Sig. Proc.*, no. 4, pp. 348–358, Mar. 2003.

[23] N. Patwari, A. Hero III, M. Perkins, N. Correal, and R. O'Dea, "Relative location estimation in wireless sensor networks," *IEEE Trans of Signal Processing*, vol. 51, no. 8, 2003.

[24] A. Savvides, W. Garber, S. Adlakha, R. Moses, and M. B. Srivastava, "On the error characteristics of multihop node localization in ad-hoc sensor netwoks," in *2nd Intl. Workshop on Inform. Proc. in Sensor Networks*, April 2003.

[25] A. Catovic and Z. Sahinoglu, "The Cramér-Rao bounds of hybrid TOA/RSS and TDOA/RSS location estimation schemes," *IEEE Commun. Lett.*, vol. 8, no. 10, pp. 626–628, Oct. 2004.

[26] N. Patwari, J. Ash, S. Kyperountas, R. M. Moses, A. O. Hero III, and N. S. Correal, "Locating the nodes: Cooperative localization in wireless sensor networks," *IEEE Signal Process. Mag.*, vol. 22, no. 4, pp. 54–69, July 2005.

[27] N. Patwari and P. Agrawal, "Effects of correlated shadowing: Connectivity, localization, and RF tomography," in *ACM/IEEE Information Processing in Sensor Networks (IPSN)*, April 2008.

[28] D. Mallants, B. P. Mohanty, A. Vervoort, and J. Feyen, "Spatial analysis of saturated hydraulic conductivity in a soil with micropores," *Soil Technology*, 1997.

[29] N. A. Cressie, *Statistics for Spatial Data*. John Wiley and Sons Inc., 1991.

[30] K. Worsley, A. Evans, S. Strother, and J. Tyler, "A linear spatial correlation model, with applications to positron emission tomography," *Journal of the American Statistical Association*, vol. 86, no. 413, pp. 55–67, March 1991.

[31] B.D.Ripley, *Spatial Statistics*. Wiley Series in Probability and Mathematical Statistics, 1981.

[32] G. D. Durgin, T. S. Rappaport, and H. Xu, "Measurements and models for radio path loss and penetration loss in and around homes and trees at 5.85 GHz," *IEEE Trans. Communications*, vol. 46, no. 11, pp. 1484–1496, Nov. 1998.

[33] J. Robinson, R. Swaminathan, and E. W. Knightly, "Assessment of urban-scale wireless networks with a small number of measurements," *MobiCom '08: Proc. 14th ACM Int'l Conf. Mobile Computing and Networking*, Sept. 2008.

[34] A. Coulson, A. G. Williamson, and R. G. Vaughan, "A statistical basis for lognormal shadowing effects in multipath fading channels," *IEEE Trans. Veh. Tech.*, vol. 46, no. 4, pp. 494–502, April 1998.

[35] P. Agrawal and N. Patwari. Link shadow correlation model calculation code. Matlab code for public download. [Online]. Available: http://span.ece.utah.edu

[36] "MPR-MIB users manual," Crossbow Technology Inc, June 2006, revision B.

[37] "TEP 123 : Collection tree protocol," http://www.tinyos.net/tinyos-2.x/doc/html/tep123.html, August 2006.

[38] W. W. Hines, D. C. Montgomery, D. M. Goldsman, and C. M. Borror, *Probability and Statistics in Engineering*, 4th ed., 2003.

IX. Appendix

Here we present the derivation of the probability $P[\mathcal{A} \cap \mathcal{B}]$ for the case of correlated shadowing given in (28). From (20), we note that $\beta_{i,j}$, $\beta_{j,k}$ and $\beta_{i,k}$ are joint Gaussian random variables. Thus the conditional distributions, $f(\beta_{i,j}|\beta_{i,k} = b)$ and $f(\beta_{j,k}|\beta_{i,k} = b)$, are also Gaussian. From the measurement data the link pair (i, j) and (j, k) of Fig. 7 are observed to have very small or no correlation between them (see link pair geometry #4 in Table I). Thus the joint distribution, $f(\beta_{i,j}, \beta_{j,k}|\beta_{i,k} = b)$, can be approximated as:

$$f(\beta_{i,j}, \beta_{j,k}|\beta_{i,k} = b) \approx f(\beta_{i,j}|\beta_{i,k} = b) f(\beta_{j,k}|\beta_{i,k} = b). \tag{29}$$

The joint distribution of $\beta_{i,j}$, $\beta_{j,k}$ and $\beta_{i,k}$, $f(\beta_{i,j}, \beta_{j,k}, \beta_{i,k})$, can be simplified using (29) and can be written as:

$$f(\beta_{i,j}, \beta_{j,k}, \beta_{i,k}) \approx f(\beta_{i,j}|\beta_{i,k} = b) f(\beta_{j,k}|\beta_{i,k} = b) f(\beta_{i,k}). \tag{30}$$

The probability $P[\mathcal{A} \cap \mathcal{B}]$ can be written in terms of joint distribution as,

$$\begin{aligned} P[\mathcal{A} \cap \mathcal{B}] &= P[\{\beta_{i,j} > 0\} \cap \{\beta_{j,k} > 0\} \cap \{\beta_{i,k} > 0\}], \\ &= \int_{\{\beta_{i,j}>0\}} \int_{\{\beta_{j,k}>0\}} \int_{\{\beta_{i,k}>0\}} \\ &\quad f(\beta_{i,j}|\beta_{i,k}) f(\beta_{j,k}|\beta_{i,k}) f(\beta_{i,k}) d\beta_{i,j} d\beta_{j,k} d\beta_{i,k}, \\ &= \int_{\beta_{i,k}>0} \left[\mathrm{Q}\left(-\mu_1/\rho_1\right)\right]^2 e^{-\frac{(\beta_{i,k}-\bar{\beta}_{i,k})^2}{2}} d\beta_{i,k}, \end{aligned} \tag{31}$$

where $\mu_1 \triangleq \underline{\mathrm{E}[\{\beta_{i,j}|\beta_{i,k}\}]} = \bar{\beta}_{i,j} + (\beta_{i,k} - \bar{\beta}_{i,j} + \kappa)\rho_{X_{i,j},X_{i,k}}$ and $\rho_1 = \sqrt{1 - \rho^2_{X_{i,j},X_{i,k}}}$.

Note that for the link pairs geometry considered, $\rho_{X_{j,k},X_{i,k}} = \rho_{X_{i,j},X_{i,k}}$ which results in the square of $\mathrm{Q}(.)$ in (31).